

The Reynolds wave shear stress in partially reflected waves

F. Addona^a, A. Lira Loarca^b, L. Chiapponi^a, M. A. Losada^b, S. Longo^a

^{a1}Dipartimento di Ingegneria e Architettura (DIA), Università di Parma, Parco Area delle Scienze, 181/A, 43124 Parma, Italy

^{b1}Instituto Interuniversitario de Investigación del Sistema Tierra, Universidad de Granada, Avda. del Mediterráneo s/n, 18006 Granada, Spain

Abstract

Wind-waves play a relevant role in the downward flux of mass, momentum and heat, and in their balances. Thus, they are quite significant in small- and large-scale processes like global warming, especially in continental shelf. There is still no consensus on the effectiveness of different mechanisms in enhancing, e.g., the carbon dioxide (CO_2) uptake in the continental shelves with respect to the open ocean. To our best knowledge, the role of partial reflections of short and long waves in the budget has been largely neglected without a specific justification, even though reflection in water waves is a recurring phenomenon. Presumably, this is a consequence of the difficulties in performing experiments with variable reflection coefficient and phase shift of the waves approaching coastal structures. We report experiments on the vertical momentum transfer in partially reflecting waves propagating on a flat horizontal bottom. We measured the free surface level and the fluid velocity, and estimated the Reynolds wave-generated shear stress. A set of experiments using paddle waves or a paddle plus wind waves and a reflection coefficient ranging from 0.10–0.75, with a phase shift of $\pi/4 - \pi$ rad, confirms the theoretical model. The results indicate that reflection must be carefully considered in the correct interpretation of data, particularly when considering momentum transfer in the vertical. The new contributions in the paper are (i) the adoption of a generation-absorption system that controls the reflection coefficient and phase shift between incident and reflected waves; (ii) the quantification of the phase shift influence on the vertical momentum transfer and its horizontal variability; (iii) the consequences for locally-generated wind-waves and wind generated surface currents. To our knowledge, these are the first experiments where the characteristics of the reflected waves have been imposed, allowing a thorough analysis of their effects on the flow field.

Keywords: partial reflection, momentum transfer, laboratory experiments, continental shelves

1. Introduction

Reflection and partial reflection of waves, wave groups, infra gravity waves, long waves are widespread and diffused in coastal regions and, more broadly, in continental shelf areas. In fact, in the continental shelf sediment transport, bed forms morphology and chemical exchanges, both in the sea-bed interface and in the air-sea interface to and from the atmosphere, play major roles in the overall scenario.

The role of continental shelves in the global cycles of several chemicals, like carbon dioxide (CO_2), is widely recognised as important and is subject to numerous analyses [e.g., 10]. The carbon cycle has been influenced by human activities and from changes of the fluxes at the air-sea interface, in particular near the coasts [20]. The quantification of the changes is generally subject to a large uncertainty (50-100%) [5], due to the numerous phenomena influencing the balance and to the reduced accuracy of field measurements, in particular in the Arctic shelves areas. The regional studies on CO_2 balance are highly dispersed, due, e.g., to non-homogeneity in the definitions of continental shelf and to different methodologies used in these studies. However, even taking into account the relevant data dispersion, bulk evaluations indicate that the average flux densities in the continental shelf area (-0.7 to $-1.2 \text{ mol C m}^{-2} \text{ yr}^{-1}$) are higher than in the open ocean ($-0.5 \text{ mol C m}^{-2} \text{ yr}^{-1}$) [14]. This trend has been confirmed by more sophisticated approaches, where the balance of CO_2 is obtained by including direct surface ocean CO_2 measurements, atmospheric CO_2 , in a model with gas transfer inferred from wind speed, salinity and temperature. These last recent models [see 14] confirm that sink of CO_2 in the continental shelf areas is larger than in open ocean (up to 40%, with an estimated uncertainty of less than 30%).

In general, there is still no consensus about many aspects involved in continental shelf areas budget of CO₂. The adoption of a global model is limited by the low grid resolution for simulating many processes, since coarse-resolution global models fail in reproducing coastal-ocean circulation [11], upwelling, coastal currents, which affect the variability of air-sea CO₂ fluxes in these areas [6, 13]. Notice that reflection, in natural environments, is always partial reflection and often takes place in the coastal areas and generally in the continental shelf areas for long waves. We infer that partially-reflected waves play a role in the circulation and locally affect carbon dioxide (and other chemicals) exchanges.

Reflection also contributes to the structural change of the bottom boundary layer in shallow water, with consequent effects on sediment transport and on bed forms. Partial reflection introduces a further scale in a flow field already controlled by several effects [29], and may cause toe erosion and the generation of rhythmic bed forms [28]. The interaction between incoming and reflected wave trains can modify the sediment transport mechanism. This event eventually enhances scouring and favors the failure of break waters and protective structures [2]. In the real world, breakwaters and sea-walls always generate wave reflection (rubble-mound breakwaters generally reflect approximately 30–40%, vertical break-waters always higher than 70%), thus partial reflection and its effects are almost ubiquitous. Non-linear waves modulated by partial reflection, and currents (always present in the field) change the intensity of sediment transport [26].

In the past decades numerous researchers have performed the analysis of vertical momentum transfer in sea gravity waves in different conditions, with waves subject to growth due to the wind action, to shoaling or to decay. This transfer is quite important to describe the flow field and to quantify all the exchanges inside the water column and at the interface with the air. Wave growth mechanism in the presence of wind has been long debated [24, 22, 18]. Whatever is the action of the wind (tangential stress, fluctuating pressure and resonance phenomena), a net transfer of momentum from the air side toward the water is expected.

The general description of the flow field takes advantage of the triple decomposition [see 25] in the sense of [30]. The variables of interest are split in a time-averaged, a periodic (organized) and a fluctuating (turbulent) component, e.g., $u = \bar{u} + \tilde{u} + u'$ for the horizontal velocity, and $w = \bar{w} + \tilde{w} + w'$ for the vertical velocity. The fluctuating component is calculated as the difference between the raw signal and the sum of the time average and of the phase average terms. By combining these expressions in the horizontal momentum equation and time averaging, it results that the shear stress in the vertical is the combination of several covariances between the velocity components. Among them, we are specifically interested in the term $-\overline{\tilde{u}\tilde{w}}$, herein defined Reynolds wave(-generated) shear stress, which in the present experiments is more than one order of magnitude larger than the turbulent shear stress $-\overline{u'w'}$. In progressive waves advancing on a flat horizontal bottom without source or sink of energy, the term $-\overline{\tilde{u}\tilde{w}}$ is null, since \tilde{u} and \tilde{w} are in quadrature. In dissipative water waves [9] the change of wave conditions in the direction of propagation gives an out-of-quadrature contribution to $-\overline{\tilde{u}\tilde{w}}$, which is used to explain the fluxes of energy and the efficiency of vertical momentum exchange. In particular, the vertical profile of the Reynolds wave shear stress is linear for dissipation near the surface and near the bottom. The sloping bottom also acts inducing a linear profile of the Reynolds wave shear stress [8]. [27] analyzed the contribution of various sources to $-\overline{\tilde{u}\tilde{w}}$ and gave an interpretation of this term by introducing the oscillatory vorticity $\overline{\tilde{w}\tilde{\omega}}$ ($\tilde{\omega}$ is orthogonal to the plane of u and w). Their results collapse to the results of other researchers for irrotational flows. See also the analysis in [7] for irregular shoaling waves.

A recent paper by [23] is focused on Reynolds wave-generated shear stress in wind-generated waves. The Authors describe some contradicting experimental results in literature, showing variegated data on the contribution of the Reynolds wave shear stress to the momentum transfer under wind generated waves. They suggest the reflection effects as responsible of varying sign and magnitude of the experimental values of $-\overline{\tilde{u}\tilde{w}}$, in addition to possible contamination due to recirculation cells in the experimental channels. However, they do not consider the phase and their results are horizontally averaged.

In this research we analyze the Reynolds wave shear stress in a flow field where a partial reflection takes place. We separate the role of the module of the reflection coefficient K_r , of the phase shift and the contribution, if any, of the local generated wind wave (period, length and height, and if it is breaking or not) and of the water surface current. This flow field is quite diffuse in nature, since porous structures, beaches, uneven bottom, are all sources of reflected waves, but it is quite complex to reproduce in the laboratory since the variation of the reflection coefficient requires a change of the end wall characteristics of the flume, and the control of the phase shift is almost impossible to realize. We take advantage of a two-paddle flume recently installed in Granada, where the paddle control allows a variation of

the reflection coefficient from zero to unity, also in presence of wind and with current recirculation, offering numerous combinations of flow conditions. Here we analyze regular waves without or with wind action. The extension to random waves and to waves plus currents is left for future work.

We remark the importance of our laboratory data, since the same type of information is hard to be obtained in the field, due e.g. the complex pattern of natural waves or to the structure of the reflecting elements.

The paper is structured as follows. In Section 2 the theoretical problem is set, evaluating the covariance \overline{uw} and the radiation stress component useful for estimating the mean water level profile. In Section 3 the experimental set-up and the procedure for executing the experiments are illustrated, while in Section 4 the measured covariances and mean water levels are compared with theory. The conclusions are reported in Section 5.

2. Theory

2.1. Wave induced Reynolds stress for regular reflected waves in uniform depth

In this section we consider only the (potential) wave-induced terms mainly following the approach by [12]. The potentials of intersecting waves can be expressed by the sum of the independent potentials for linear theory. However, non-linear theory requires a more in-depth analysis to include the interaction terms, often described as “bound” waves. The potential and the free surface elevation of two trains of finite amplitude waves propagating in the opposite direction are

$$\Phi = \Phi_i + \Phi_r + \Phi_b, \quad \eta = \eta_i + \eta_r + \eta_b, \quad (1)$$

where i , r and b stand for “incident”, “reflected” and “bound”, respectively. The potential and the free surface elevation are expanded in series as

$$\Phi_i = a\Phi_i^{(0)} + a^2\Phi_i^{(1)}, \quad \Phi_r = K_r a\Phi_r^{(0)} + K_r^2 a^2\Phi_r^{(1)}, \quad \Phi_b = a^2\Phi_b^{(1)}, \quad (2)$$

$$\eta_i = a\eta_i^{(0)} + a^2\eta_i^{(1)}, \quad \eta_r = K_r a\eta_r^{(0)} + K_r^2 a^2\eta_r^{(1)}, \quad \eta_b = a^2\eta_b^{(1)}, \quad (3)$$

where K_r is the ratio of the reflected wave amplitude to the incident wave amplitude, and a is the incident wave amplitude. The incident and the reflected waves satisfy the classical differential problem

$$\left. \begin{array}{l} \Phi_{,xx} + \Phi_{,zz} = 0, \quad -h < z < \eta, \quad \forall x, \\ g\eta + \Phi_{,t} + \frac{1}{2}[(\Phi_{,x})^2 + (\Phi_{,z})^2] \quad \text{on } z = \eta, \\ \Phi_{,z} = \eta_{,t} + \eta_{,x}\Phi_{,x} \quad \text{on } z = \eta, \\ \Phi_{,z} = 0 \quad \text{on } z = -h, \end{array} \right\} \quad (4)$$

with the additional conditions

$$\int_0^{2\pi/k} \eta(x, t) dx = 0, \quad (5)$$

$$\nabla\Phi(x, z, t + 2\pi/\omega) = \nabla\Phi(x + 2\pi/k, z, t) = \nabla\Phi(x, z, t), \quad (6)$$

where x is the horizontal coordinate, z is the vertical coordinate positive upward with the origin at the still water level ($z = -h$ is the horizontal bottom), t is the time, g is gravity acceleration, $k = 2\pi/L$ is the wave number, L is the wave length, $\omega = 2\pi/T$ is the angular frequency and T is the wave period. The comma in the subscript indicates the partial derivative. The solution to the second order is

$$\begin{aligned} \Phi_j = \frac{a_j \omega_j}{k_j} \frac{\cosh[k_j(z + h)]}{\sinh(k_j h)} \sin(k_j x - \omega_j t + \varphi_j) + \\ \frac{3a_j^2 \omega_j}{8} \frac{[\coth^4(k_j h) - 1] \cosh[2k_j(z + h)]}{\cosh(2k_j h)} \sin[2(k_j x - \omega_j t + \varphi_j)] - \frac{a_j^2 \omega_j^2}{4 \sinh^2(k_j h)} t, \end{aligned} \quad (7)$$

for the potential, and

$$\eta_j = a_j \cos(k_j x - \omega_j t + \varphi_j) + \frac{a_j^2}{4k_j} [3 \coth^3(k_j h) - \coth(k_j h)] \cos[2(k_j x - \omega_j t + \varphi_j)], \quad (8)$$

for the elevation, where $j = i, r$, φ_j is a phase shift and the dispersion relation $\omega_j^2 = gk_j \tanh(k_j h)$ holds. Eqs (7–8) can be specialized for the incident and for the reflected wave component by imposing that $k_i = -k_r \equiv k$, $a_r = K_r a_i$, $\omega_i = \omega_r \equiv \omega$ and specifying the phase shift φ_i and φ_r , respectively. We also define $\theta_i = kx - \omega t + \varphi_i$ and $\theta_r = kx + \omega t - \varphi_r$, with $\theta_i + \theta_r = 2kx + \varphi_i - \varphi_r$ and $\theta_r - \theta_i = 2\omega t - \varphi_i - \varphi_r$.

The bound wave potential and elevation is obtained by imposing that the potential and the elevation in eq. (1), with components expressed by (2–3), satisfy the differential problem (4) and the conditions (5–6). The result to second order is (to the first order is null)

$$\Phi_b = \frac{K_r a_i^2 \omega}{4} [3 + \coth^2(kh)] \sin(\theta_r - \theta_i), \quad \eta_b = K_r k a_i^2 \coth(2kh) \cos(\theta_i + \theta_r). \quad (9)$$

We notice that the potential of the bound wave (Φ_b) does not contribute to the velocity field (it depends only on t) and that the bound wave (η_b) is stationary. By differentiating the potential, the horizontal and vertical velocities are computed:

$$\begin{aligned} \tilde{u}(x, z, t) \equiv \Phi_{,x} &= \frac{g a_i k}{\omega} \frac{\cosh[k(z+h)]}{\cosh(kh)} (\cos \theta_i - K_r \cos \theta_r) + \\ &\quad \frac{3 g a_i^2 k^2}{4 \omega} \frac{\cos[2k(h+z)]}{\cosh(kh) \sinh^3(kh)} [\cos(2\theta_i) - K_r^2 \cos(2\theta_r)], \end{aligned} \quad (10)$$

$$\begin{aligned} \tilde{w}(x, z, t) \equiv \Phi_{,z} &= \frac{g a_i k}{\omega} \frac{\sinh[k(z+h)]}{\cosh(kh)} (\sin \theta_i - K_r \sin \theta_r) + \\ &\quad \frac{3 g a_i^2 k^2}{4 \omega} \frac{\sinh[2k(h+z)]}{\cosh(kh) \sinh^3(kh)} [\sin(2\theta_i) - K_r^2 \sin(2\theta_r)], \end{aligned} \quad (11)$$

where the tilde indicates wave orbital velocity. The instantaneous free surface level is

$$\begin{aligned} \eta(x, t) &= a_i (\cos \theta_i + K_r \cos \theta_r) + \frac{k a_i^2}{4} [3 \coth^3(kh) - \coth(kh)] \times \\ &\quad [\cos(2\theta_i) + K_r^2 \cos(2\theta_r)] + K_r k a_i^2 \coth(2kh) \cos(\theta_r + \theta_i). \end{aligned} \quad (12)$$

Considering only the linear contribution (the first term on the r.h.s.), nodes and antinodes can be detected at $x_n = mL/4 - (\varphi_i - \varphi_r)L/(4\pi)$, and $x_a = mL/2 - (\varphi_i - \varphi_r)L/(4\pi)$, $m = 0, 1, 2, \dots$; the second order and the bound wave contributions render the nodes and the antinodes fluctuating around the sections at x_n and x_a . Time averaging the covariance $-\overline{uw}$ from eqs (10–11) yields

$$-\overline{uw} = K_r g k a_i^2 \frac{\sinh[2k(z+h)]}{\sinh(2kh)} \sin(\theta_i + \theta_r) + \frac{9}{16} K_r^2 g k^3 a_i^4 \frac{\sinh[4k(h+z)]}{\sinh^6(kh) \sinh(2kh)} \sin(2\theta_i + 2\theta_r). \quad (13)$$

In presence of reflection the covariance is different from zero, with maximum values achieved for $K_r \rightarrow 1$ (perfect reflection). Moreover, there is a spatial variation of $-\overline{uw}$ which supports a mean water level variation. The radiation stress can be used for estimating the mean water level.

2.2. The radiation stress for regular reflected waves in uniform depth and the mean water level

Following [19] we evaluate the component S_{xx} of radiation stress as

$$S_{xx} = \overline{\int_{-h}^{\zeta} \rho \tilde{u}^2 dz} + \overline{\int_{-h}^0 (p - p_0) dz} + \overline{\int_0^{\zeta} pdz} \equiv S_{xx}^{(1)} + S_{xx}^{(2)} + S_{xx}^{(3)}, \quad (14)$$

where $\zeta = \bar{\zeta} + \eta$ and $\bar{\zeta}$ is the mean water level. Upon evaluating all terms in eq. (14) up to second order yields

$$S_{xx} = E \left(G + \frac{1}{2} \right) (1 + K_r^2) - EGK_r \cos(\theta_i + \theta_r) \cosh(2kh) + \rho gh \bar{\zeta}, \quad (15)$$

where $E = \rho g a_i^2 / 2$ is the energy density of the incident wave and $G = 2kh / \sinh(2kh)$. S_{xx} must be equal to its horizontal average over a wavelength since momentum cannot accumulate, thus eq. (15) reduces to $S_{xx} = E(G + 1/2)(1 + K_r^2)$. For progressive waves the reflection coefficient is null ($K_r \rightarrow 0$), and it yields $S_{xx} = E(G + 1/2)$. For standing waves with perfect reflection ($K_r \rightarrow 1$) it yields $S_{xx} = 2E(G + 1/2)$, which recovers the result in [19]. The mean water level is computed by imposing the balance between the two last terms on the r.h.s of eq. (15):

$$\bar{\zeta} = ka_i^2 K_r \coth(2kh) \cos(\theta_i + \theta_r) + \text{const} \equiv \eta_b + \text{const}, \quad (16)$$

where the constant can be evaluated by imposing mass conservation in the channel. See also [21] for wave induced mean quantities with permeable submerged breakwaters, where the mean water level is raised at the antinodes and lowered at the nodes. In the limit $K_r \rightarrow 1$ and $\phi_i = \phi_r$, eq. (16) reduces to the expression given in [19].

3. Experiments

In order to verify the theory, several experiments were conducted in the Atmosphere-Ocean Interaction Flume (CIAO) at IISTA (Instituto Interuniversitario de Investigación del Sistema Tierra). The CIAO is a wave flume 100 cm wide, 1600 cm long and 70 cm deep. It allows the generation of regular waves (up to second order) and irregular waves with period from 1 to 5 s and height up to 25 cm. A closed-circuit wind-generation system (wind tunnel) with wind speed up to 12 m s⁻¹ directly generates waves with an effective fetch length approximately equal to 1000 cm; a current-generation system allows currents up to 75 cm s⁻¹. A main feature is the presence of two paddles at the opposite sides controlled by a software for the complete absorption or for a partial reflection of waves, including a possible phase shift of the reflected wave. All the actions can be made in both direction (except for the wind generation) and are controlled independently from each other.

For the present experiments, paddle waves and paddle plus wind waves were generated, taking advantage of the control system for changing the reflection coefficient and the phase shift of the reflected component. Figure 1 shows the experimental set-up. Eight UltraLab ULS 80D acoustics wave gauges were employed for water level measurements along the flume, with a maximum repetition rate equal to 75 Hz, a declared space resolution of 0.18 mm and a reproducibility of $\pm 0.15\%$. Measurements of the wind speed were performed with a Pitot tube in the LDV section, at ten different levels in the vertical in air and for each angular speed of the fan adopted in the tests. The signal was acquired for ≈ 60 s with a data rate of 1 kHz. Measurements of fluid velocity in the water side were performed with a two-component Laser Doppler Velocimeter by TSI Inc., with fiber-optics probe, moved in the horizontal (x) and vertical (z) directions by a PC controlled traverse system. Water was seeded with glass particles and measurements were taken in ten points in the vertical for each section, with data rates from hundreds to over a thousand hertz. Further details on LDV and traverse system used can be found in [17].

3.1. Data analysis

Velocities measured by LDV are analyzed decomposing the data into the time average $\bar{u}(x, z) = (1/N_{acq}) \sum u(x, z, t)$ where N_{acq} is the number of samples. The periodic (organized) velocity is obtained by phase averaging the raw signal, after subtracting the time average term, $\tilde{u}(x, z, t) = \langle u - \bar{u} \rangle = (1/N_w) \sum_{n=1}^{N_w} [u(x, z, t + nT) - \bar{u}(x, z)]$, $0 \leq t < T$, where T is the regular wave period and N_w is the number of waves. The fluctuating term is the difference between the raw signal and the sum of the time average and of the phase average. The reflection coefficient K_r , the phase shift $\varphi_i - \varphi_r$ and the height of incident waves are estimated by using the Baquerizo's method [see 1]. In the present analysis the three sensors used to estimate the reflection parameters were taken adjacent to the LDV measurement points. The wave period T is the theoretical value imposed by the paddle (and further checked with a zero crossing analysis). The wavelength L derives from the linear dispersion relation $\omega^2 = gk \tanh(kh)$.

Free surfaces levels are acquired during all the LDV measurements belonging to each vertical profile, hence numerous independent realizations of the same experiment are available. It allows the evaluation of the statistical

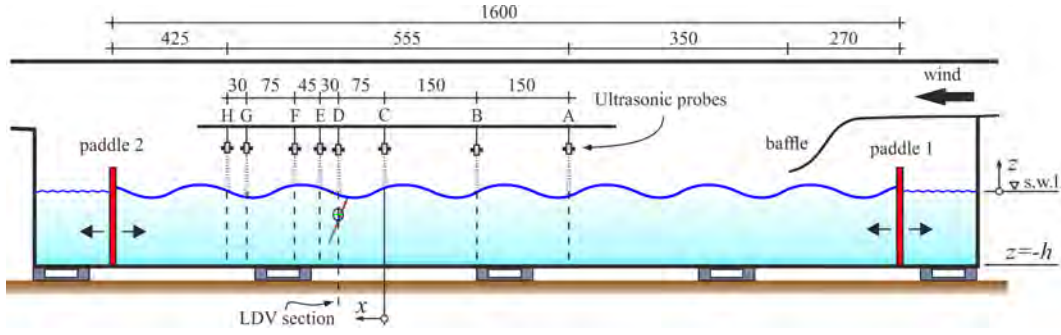


Figure 1: A sketch of the experimental set-up with the instruments layout. For the present experiments, paddle 1 was used for generation and paddle 2 for active reflection control.

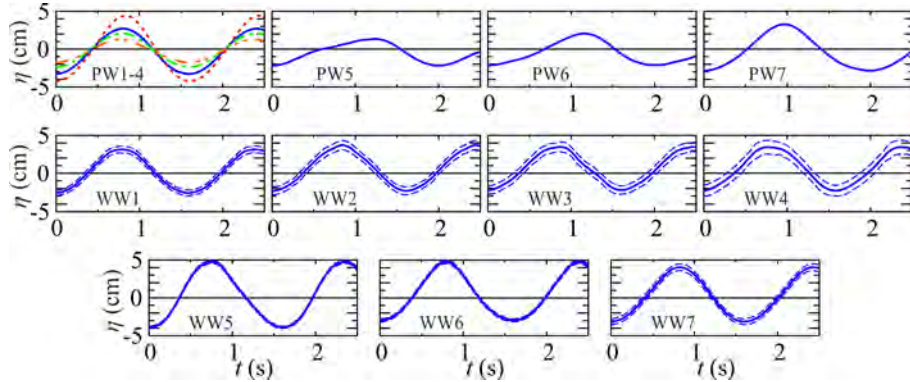


Figure 2: The phase-averaged free surface levels measured at the LDV measurements section. The dashed curves are the phase average \pm one standard deviation.

estimators of the wave characteristics as true ensemble averages. The confidence bands of the theoretical Reynolds wave shear stress are evaluated through a Montecarlo simulation. Each measurement lasted ≈ 330 s, a time interval sufficient for achieving the consistency of the second order statistical estimators.

4. Experimental results

The experiments are listed in Table 1, with parameters computed through the statistical analysis of the water elevation measurements. All the velocities are scaled with respect to $H_t T^{-1}$, where T is the regular wave period and H_t the total height. When LDV is co-located with a wave gauge, H_t represents root mean square value H_{rms} from the statistics of the corresponding sensor. In different sections H_t is calculated as [see 4, 3]:

$$H_t = H_{irms} \sqrt{1 + K_r^2 + 2K_r(2kx + \varphi_i - \varphi_r)}, \quad (17)$$

where H_{irms} is the root-mean-squared height of the incident wave. Figure 2 shows the phase averaged surface levels for all the experiments. The variability of the wave profile is generally limited for paddle waves, which have standard deviation of less than a tenth millimeter. It is more evident in presence of wind, which have standard deviation of several millimeters. An increasing asymmetry between crest shape and trough shape is also evident for increasing H_t/L , see Figure 2. The horizontal mean velocity (not shown) is negative and $\approx 0.5H_t T^{-1}$ for most experiments. As expected, in presence of wind, the horizontal velocity is positive, i.e. cocurrent with the wind near the free surface. The wind waves superimposed to the paddle waves (not shown) have a wave length of less than ≈ 10 cm, thus their orbital motion has effects for ≈ 5 cm, less than 10% of the water column.

Expts	U_{ref} (m s ⁻¹)	x (cm)	H_i (cm)	H_t (cm)	T (s)	K_r	$\Delta\varphi$ (rad)
PW1	0	70	5.5 ± 0.1	6.1 ± 0.1	1.6	0.108 ± 0.002	3.14 ± 0.04
2 ^p	0	76	7.5 ± 0.3	8.6 ± 0.1	1.6	0.325 ± 0.004	2.23 ± 0.02
3a	0	76	5.7 ± 0.1	4.5 ± 0.1	1.6	0.272 ± 0.004	0.91 ± 0.03
4	0	76	5.9 ± 0.2	3.0 ± 0.1	1.6	0.556 ± 0.004	0.69 ± 0.04
5 ^s	0	76	7.9 ± 0.1	3.6 ± 0.1	2.0	0.743 ± 0.001	0.72 ± 0.01
6 ^s	0	76	7.4 ± 0.1	4.2 ± 0.1	2.0	0.495 ± 0.002	0.83 ± 0.01
7 ^s	0	76	7.1 ± 0.1	6.1 ± 0.1	2.0	0.175 ± 0.003	1.4 ± 0.1
3b	0	122	5.7 ± 0.1	6.7 ± 0.1	1.6	0.253 ± 0.006	0.87 ± 0.09
3c	0	105	5.6 ± 0.1	5.7 ± 0.1	1.6	0.249 ± 0.003	0.86 ± 0.01
3d	0	90	5.6 ± 0.1	5.2 ± 0.1	1.6	0.247 ± 0.009	0.94 ± 0.09
3e	0	58	5.6 ± 0.1	4.2 ± 0.1	1.6	0.254 ± 0.003	0.93 ± 0.05
WW1	3.65	70	5.2 ± 0.4	6.2 ± 0.1	1.6	0.113 ± 0.007	2.97 ± 0.09
2	5.14	70	5.4 ± 0.1	6.4 ± 0.1	1.6	0.118 ± 0.007	2.9 ± 0.1
3	5.88	70	5.3 ± 0.1	6.2 ± 0.1	1.6	0.110 ± 0.01	2.67 ± 0.06
4	6.62	70	5.5 ± 0.1	6.5 ± 0.1	1.6	0.114 ± 0.007	2.58 ± 0.03
5 ^p	4.85	76	7.6 ± 0.1	8.9 ± 0.1	1.6	0.34 ± 0.01	2.23 ± 0.02
6 ^p	5.78	76	7.2 ± 0.1	8.1 ± 0.1	1.6	0.295 ± 0.004	2.05 ± 0.02
7 ^p	7.65	76	6.9 ± 0.1	7.9 ± 0.1	1.6	0.299 ± 0.004	1.95 ± 0.01

Table 1: Parameters of the experiments, PW stands for “paddle generated waves” and WW stands for “wind plus paddle generated waves”. U_{ref} is the air velocity measured by a Pitot, H_i is the incoming wave height, H_t is the total wave height as defined in eq. (17), T is the period of the paddle oscillation, K_r and $\Delta\varphi = \varphi_i - \varphi_r$ are the reflection coefficient and the phase lag, respectively. LDV measurements at $x = 70 - 76$ cm. Expts PW3a–e refer to the same experimental set-up but with fluid velocity measured in sections ($x = 76, 122, 105, 90, 58$ cm, respectively). p and s indicate a passive absorption and a second order generation, respectively. All the other experiments were with a first order generation and an active absorption system.

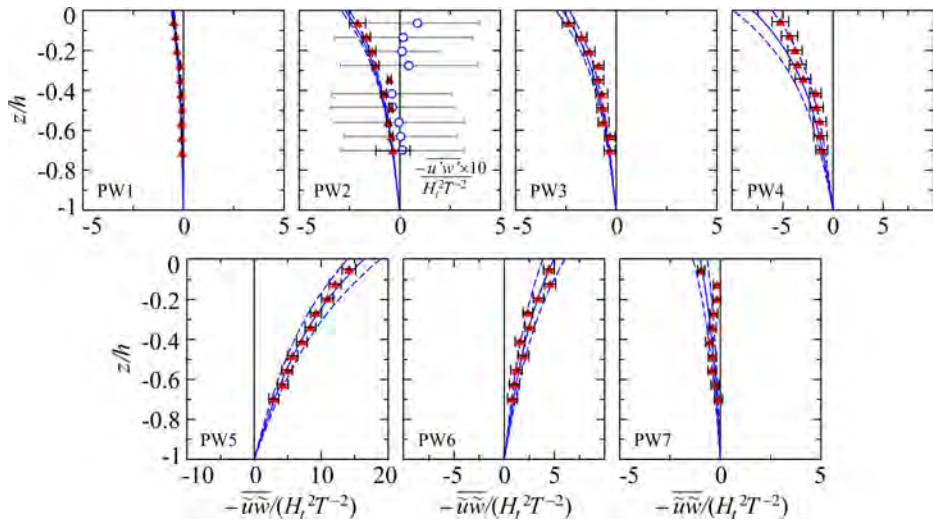


Figure 3: Expts PW1–7, paddle waves. Comparison between measured (triangles) and theoretical (solid lines) covariances $-\bar{uw}$ non dimensional with respect to the total local wave height H_t , including incident and reflected wave trains and taking into account the phase shift. For Expt PW2 also Reynolds turbulent shear stress (circles) is shown, note the different scale. Dashed lines and bars represent 95% confidence limits.

4.1. Vertical and horizontal variability of the Reynolds wave shear stress $-\bar{uw}$

Figures 3–4 show the theoretical and experimental values of $-\bar{uw}$ for paddle waves and paddle plus wind waves, respectively. The agreement is fairly good, with overlap between the error bars and the 95% confidence limits for the great majority of the experimental points. It is clear that for paddle waves the combination of experimental parameters gives both positive and negative values of the covariance. For paddle waves plus wind the values are only negative but we expect that a different section of measurements would have given also positive values. We notice that the Reynolds turbulent shear stress (shown only for Expts PW2 and WW2; note that it is on a different scale) is much smaller than the Reynolds wave shear stress, i.e. at least one order of magnitude. It should be true far from the free surface, where turbulence related to free surface fluctuations even without breaking can be dominant [see 15, 16]. We remark the fact that, following the structure of eq. (13), the vertical profile of the Reynolds wave shear stress can assume positive or negative values. Furthermore it is predictable by theory, depending on the reflection parameters and on the section of the velocity measurements along the channel (coordinate x). It explains why some test shows a negative profile, while others (like PW5 and PW6) exhibit positive vertical profiles.

A further assessment of our model is obtained by repeating velocity measurements at different sections x for a single experiment. Figure 5 shows the spatial variability along x of the covariance $-\bar{uw}$ for test PW3a–e at different levels z . This is a clear indication that the section of measurement modulates the value and the sign of the Reynolds wave shear stress. A last check of the model is based on the mean water level given by eq.(16). Figures 6 shows the comparison with theory of the experimental data for the paddle waves (Expts PW2–6) and for some experiments with paddle plus wind waves (Expts WW5–7), respectively. Notice that the experimental mean water level (MWL) for a finite-length channel is very hard to be evaluated. That is due to several factors. Above all, the MWL is strongly influenced by the boundary conditions due to the finite length of the channel, which is just 4–5 times the experimental wave length, while the theoretical model considers an indefinitely long channel. Furthermore, there is no feedback system to control the mass conservation, thus part of water may accumulate locally in the inner or in the outer part of the paddle position. In this sense, the comparison is again fairly good, with a peak-to-peak value well predicted and with an acceptable spatial coherence between theory and experiments.

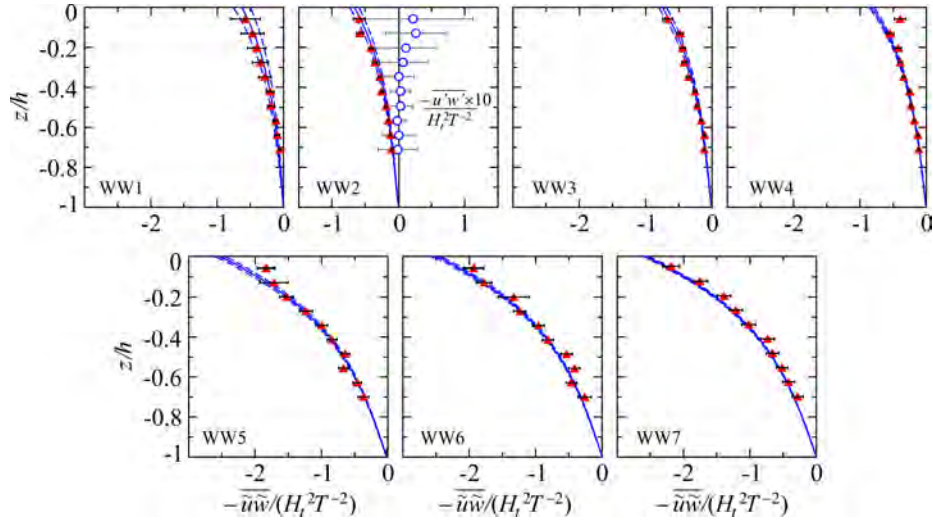


Figure 4: Expts WW1–7, paddle waves plus wind. See Figure 3 for caption.

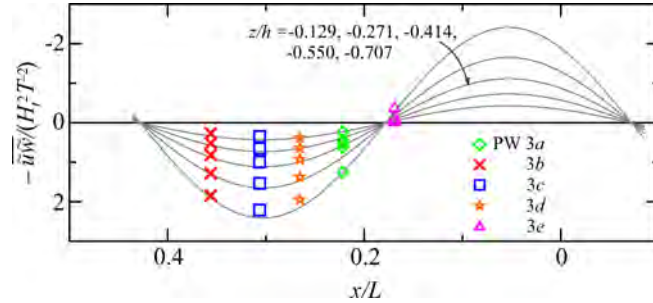


Figure 5: Spatial variability along x of the covariance $-\bar{u}\bar{w}$ at different levels z . The continuous lines are the theoretical values, the symbols refer to experiments PW3a–e. For an easy visualization only one level in two is shown.

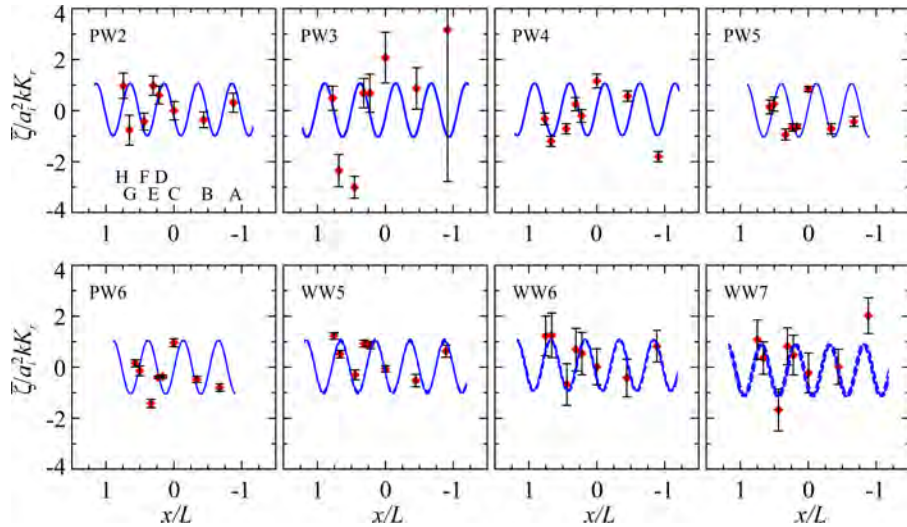


Figure 6: Mean water level measured (symbols) and theoretical value calculated by eq. (16) (solid line). The symbols A-H in the upper left panel indicate the location of the Ultrasonic gauges.

5. Discussion and Conclusions

The flume equipped with a generation-absorption system with control of the reflection coefficient and phase shift represents a step in advance in physical modeling of complex phenomena. It is a matter of evidence that controlling the flow field for a sufficient long time allows detailed measurements, difficult to obtain in standard wave flumes and in the field. Having simplified the scenario gives the tools to analyze more complex situations (the standard situations in the field), where currents, bottom effects, local morphology also contribute to the overall dynamics of water and of sediments. In particular, the sediments dynamics is strongly influenced by the (minor) effects of the composite waves (incident and partially reflected) on the bottom boundary layer. We bring in mind that bed forms are often described as the answer of the bottom to small perturbations, which eventually grow up and evolve with the shape of ripples, sandbars etc.. Hence, very small changes in the flow field can significantly alter the sand bottom evolution. We have limited the analysis to momentum transfer in the vertical, but we expect that also vorticity, diffusion, currents profiles are affected by partial reflection and phase shift. Hence, the free surface elevation modification induced by reflection is only one and not even the most relevant effect.

We have experimentally analyzed the vertical profiles and the horizontal variability of the Reynolds wave shear stress for mechanically generated waves and mechanically plus wind generated waves, in partial reflecting conditions. The analysis includes the phase shift between the incident and the reflected wave, which is a novelty.

As a caveat for experiments analysis, the technique for separating “waves” from “turbulence” becomes quite important to avoid pseudo-turbulence artifacts due to leakage from the organized to the fluctuating motion. Having clear the effects of partial reflection helps in the correct separation.

We have found that reflection plays a dominant role in modulating the Reynolds wave shear stress, which is zero only for progressive waves. Reynolds wave shear stress is usually much larger than Reynolds turbulent shear stress, even for very small reflection coefficient. As a consequence, the transport properties usually attributed to turbulence, can also be considered as a characteristic of reflected waves in a fluid domain mostly non-turbulent.

Reflection controls the spatial variability of the mean quantities and creates a sequence of alternating sign vertical profiles for the Reynolds wave shear stress. The horizontal spatial average of Reynolds wave shear stress is expected to give null contribution only if it is extended for several wave lengths and for rigorously homogeneous conditions. These conditions seldom occur in the laboratory and are absent in the field, hence a phase resolved analysis of the mean quantities is compulsory.

The expected effect on locally-generated wind-waves is an enhancement of the efficiency in energy and momentum transfer from the wind to the water.

References

- [1] BAQUERIZO, A. 1995 Reflexión del oleaje en playas. métodos de evaluación y de predicción. PhD thesis, Universidad de Cantabria, Santander.
- [2] BAQUERIZO, A. & LOSADA, M. A. 1999 Sediment transport around a mound breakwater: The toe erosion problem. In *Coastal Engineering 1998*, pp. 1720–1729.
- [3] BAQUERIZO, A. & LOSADA, M. A. 1999 Wave height to depth ratio in front of coastal structures. In *Proceedings of Coastal Structures*.
- [4] BAQUERIZO, A., LOSADA, M. A., SMITH, J. M. & KOBAYASHI, N. 1997 Cross-shore variation of wave reflection from beaches. *Journal of Waterway, Port, Coastal, and Ocean Engineering* **123** (5), 274–279.
- [5] BAUER, J. E., CAI, W.-J., RAYMOND, P. A., BIANCHI, T. S., HOPKINSON, C. S. & REGNIER, P. A. G. 2013 The changing carbon cycle of the coastal ocean. *Nature* **504** (7478), 61–70.
- [6] BORGES, A. V. 2005 Do we have enough pieces of the jigsaw to integrate CO₂ fluxes in the coastal ocean? *Estuaries* **28** (1), 3–27.
- [7] DE SERIO, F. & MOSSA, M. 2013 A laboratory study of irregular shoaling waves. *Experiments in Fluids* **54** (6), 1536.
- [8] DE VRIEND, H. J. & KITOU, N. 1991 Incorporation of wave effects in a 3D hydrostatic mean current model. In *Coastal Engineering 1990*, pp. 1005–1018. Elsevier.
- [9] DEIGAARD, R. & FREDØE, J. 1989 Shear stress distribution in dissipative water waves. *Coastal Engineering* **13** (4), 357–378.
- [10] FENNEL, K. 2010 The role of continental shelves in nitrogen and carbon cycling: Northwestern North Atlantic case study. *Ocean Science* **6** (2), 539.
- [11] FIECHTER, J., CURCHITSER, E. N., EDWARDS, C. A., CHAI, F., GOEBEL, N. L. & CHAVEZ, F. P. 2014 Air-sea CO₂ fluxes in the California Current: Impacts of model resolution and coastal topography. *Global Biogeochemical Cycles* **28** (4), 371–385.
- [12] GODA, Y. & ABE, Y. 1968 Apparent coefficient of partial reflection of finite amplitude waves. *Tech. Rep.*. Port and Harbour Research Institute.
- [13] LACHKAR, Z., ORR, J. C., DUTAY, J.-C. & DELECLUSE, P. 2007 Effects of mesoscale eddies on global ocean distributions of CFC-11, CO₂, and Δ¹⁴C. *Ocean Science* **3** (4), 461–482.
- [14] LARUELLE, G. G., LAUERWALD, R., PFEIL, B. & REGNIER, P. 2014 Regionalized global budget of the CO₂ exchange at the air-water interface in continental shelf seas. *Global Biogeochemical Cycles* **28** (11), 1199–1214.

- [15] LONGO, S. 2010 Experiments on turbulence beneath a free surface in a stationary field generated by a Crump weir: free-surface characteristics and the relevant scales. *Experiments in Fluids* **49** (6), 1325–1338.
- [16] LONGO, S. 2011 Experiments on turbulence beneath a free surface in a stationary field generated by a crump weir: turbulence structure and correlation with the free surface. *Experiments in Fluids* **50** (1), 201–215.
- [17] LONGO, S. 2012 Wind-generated water waves in a wind tunnel: Free surface statistics, wind friction and mean air flow properties. *Coastal Engineering* **61**, 27–41.
- [18] LONGUET-HIGGINS, M. S. 1969 Action of a variable stress at the surface of water waves. *The Physics of Fluids* **12** (4), 737–740.
- [19] LONGUET-HIGGINS, M. S. & STEWART, R. W. 1964 Radiation stresses in water waves; a physical discussion, with applications. In *Deep Sea Research and Oceanographic Abstracts*, , vol. 11, pp. 529–562. Elsevier.
- [20] MACKENZIE, F. T., DE CARLO, E. H. & LERMAN, A. 2011 5.10-Coupled C, N, P, and O Biogeochemical Cycling at the Land–Ocean Interface. *Treatise on estuarine and coastal science* pp. 317–342.
- [21] MÉNDEZ, F. J., LOSADA, I. J. & LOSADA, M. A. 2001 Wave-induced mean magnitudes in permeable submerged breakwaters. *Journal of Waterway, Port, Coastal, and Ocean Engineering* **127** (1), 7–15.
- [22] MILES, J. W. 1957 On the generation of surface waves by shear flows. *Journal of Fluid Mechanics* **3** (2), 185–204.
- [23] OLFAKHT, M., WARE, P., CALLAGHAN, D. P., NIELSEN, P. & BALDOCK, T. E. 2017 Momentum transfer under laboratory wind waves. *Coastal Engineering* **121**, 255–264.
- [24] PHILLIPS, O. M. 1957 On the generation of waves by turbulent wind. *Journal of Fluid Mechanics* **2** (5), 417–445.
- [25] PHILLIPS, O. M. 1966 *The dynamics of the upper oceans*. New York: Cambridge University Press.
- [26] RIBBERINK, J. S., KATOPODI, I., RAMADAN, K. A. H., KOELEWIJN, R. & LONGO, S. 1995 Sediment transport under (non)-linear waves and currents. In *Coastal Engineering 1994*, pp. 2527–2541.
- [27] RIVERO, F. J. & ARCILLA, A. S. 1995 On the vertical distribution of $\langle \tilde{u}\tilde{w} \rangle$. *Coastal Engineering* **25** (3-4), 137–152.
- [28] SÁNCHEZ-BADORREY, E., LOSADA, M. A. & RODERO, J. 2008 Sediment transport patterns in front of reflective structures under wind wave-dominated conditions. *Coastal Engineering* **55** (7-8), 685–700.
- [29] SÁNCHEZ-BADORREY, E., MANS, C., BRAMATO, S. & LOSADA, M. A. 2009 High-order oscillatory contributions to shear stress under standing regular wave groups: Theory and experimental evidence. *Journal of Geophysical Research: Oceans* **114** (C3).
- [30] THAIS, L. & MAGNADET, J. 1995 A triple decomposition of the fluctuating motion below laboratory wind water waves. *Journal of Geophysical Research: Oceans* **100** (C1), 741–755.